Piezo1, a mechanically activated ion channel, is required for vascular development in mice

Sanjeev S. Ranade[a,b,1], Zhaozhu Qiu[a,b,c,1], Seung-Hyun Woo[a,b], Sung Sik Hur[d,e], Swetha E. Murthy[a,b], Stuart M. Cahalan[a,b], Jie Xu[a,b,c], Jayanti Mathur[c], Michael Bandell[a,b,c], Bertrand Coste[a,b,2], Yi-Shuan J. Li[d,e], Shu Chien[d,e,3], and Ardem Patapoutian[a,b,3]

[a]Howard Hughes Medical Institute and [b]Department of Molecular and Cellular Neuroscience, The Scripps Research Institute, La Jolla, CA 92037; [c]Genomics Institute of the Novartis Research Foundation, San Diego, CA 92121; and [d]Department of Bioengineering and [e]Institute of Engineering in Medicine, University of California, San Diego, La Jolla, CA 92032

Contributed by Shu Chien, May 21, 2014 (sent for review May 09, 2014)

Mechanosensation is perhaps the last sensory modality not understood at the molecular level. Ion channels that sense mechanical force are postulated to play critical roles in a variety of biological processes including sensing touch/pain (somatosensation), sound (hearing), and shear stress (cardiovascular physiology); however, the identity of these ion channels has remained elusive. We previously identified Piezo1 and Piezo2 as mechanically activated cation channels that are expressed in many mechanosensitive cell types. Here, we show that Piezo1 is expressed in endothelial cells of developing blood vessels in mice. Piezo1-deficient embryos die at midgestation with defects in vascular remodeling, a process critically influenced by blood flow. We demonstrate that Piezo1 is activated by shear stress, the major type of mechanical force experienced by endothelial cells in response to blood flow. Furthermore, loss of Piezo1 in endothelial cells leads to deficits in stress fiber and cellular orientation in response to shear stress, linking Piezo1 mechanotransduction to regulation of cell morphology. These findings highlight an essential role of mammalian Piezo1 in vascular development during embryonic development.

Mechanotransduction, the conversion of physical forces into a biochemical response, is an essential signaling mechanism used by all organisms (1). Diverse physiological processes including hearing, touch, and blood pressure regulation require the ability of cells to sense and respond to mechanical stimuli (2–4). Impairment in mechanotransduction can lead to a wide range of pathologies including deafness and atherosclerosis (5, 6). The cellular response to mechanical force requires the coordinated action of multiple proteins; however, the identity of mechanotransducers in mammals remains poorly understood (7).

Classical studies from auditory sensory cells first implicated ion channels to be inherently mechanically activated (8). Since then, stretch-activated cation channels have been recorded from various tissues (9), but their identity has remained unknown (10, 11). For an ion channel to be considered a physiologically relevant transducer of mechanical stimuli, several criteria must be met (12). The ion channel must be expressed in the appropriate mechanosensitive cells, its expression should be required for mechanotransduction in an in vivo setting, and ideally the expression of the channel in a naive cell must render that cell mechanosensitive.

Progress toward identification of mechanically activated (MA) ion channels has been limited to a subset of ion channel families. In the invertebrates *Caenorhabditis elegans* and *Drosophila melanogaster*, members of the DEG/ENaC family and the TRP ion channel NOMPC have been conclusively shown to act as mechanotransduction ion channels (13–16). Mammals, however, do not have an ortholog of NOMPC, and the physiological relevance of the mammalian ENaC orthologs in mechanotransduction remains unclear. Many other TRP channels including TRPPs, TRPA1, and TRPV4 have been implicated in sensing mechanical stimuli; however, none has been shown to be required in vivo for sensing mechanical forces, nor to be necessary and sufficient for mechanotransduction (12). The two-pore potassium channels TREK-1, TREK-2, and TRAAK are mechanically activated in heterologous expression systems, and TREK-1 plays a role in modulating the mechanical sensitivity of dorsal root ganglia neurons (17). Overall, the identification of relatively few candidate genes has been a major impediment to studying mechanotransduction processes in vivo.

We recently identified Piezo proteins as pore-forming subunits of an evolutionarily conserved MA cation channel family (18). Mouse Piezo1 forms a homo-multimeric complex of ~1.2 mDa, with each monomer containing over 35 transmembrane domains (19). Piezo1 is necessary for mechanically activated currents in the Neuro2A cell line and is sufficient for conferring stretch-activated currents in heterologous cell expression. Purified mouse Piezo1 retains channel activity when reconstituted without accessory subunits into artificial lipid bilayers. The single Piezo member in *Drosophila* plays a role in sensing noxious mechanical stimuli (20), and mouse Piezo2 has been shown to be critically required for mechanotransduction in mammalian Merkel cells (21–23). Gain-of-function PIEZO1 mutations have recently been shown to cause hereditary xerocytosis in humans (24–26); however, it is still unclear whether the mammalian Piezo1 plays a role in mechanotransduction

Significance

Ion channels that are activated by mechanical force have been implicated in numerous physiological systems. In mammals, the identity of these channels remains poorly understood. We recently described Piezos as evolutionarily conserved mechanically activated ion channels and showed that Piezo2 is required for activation of touch receptors in the skin. Here we show that Piezo1 is a critical component of endothelial cell mechanotransduction and is required for embryonic development. Piezo1 is expressed in embryonic endothelial cells and is activated by fluid shear stress. Loss of Piezo1 affects the ability of endothelial cells to alter their alignment when subjected to shear stress. These results suggest a potential role for Piezo1 in mechanotransduction in adult cardiovascular function and disease.

Author contributions: S.S.R., Z.Q., S.S.H., Y.-S.J.L., S.C., and A.P. designed research; S.S.R., Z.Q., S.-H.W., S.S.H., S.E.M., S.M.C., J.X., J.M., M.B., and B.C. performed research; S.S.R., Z.Q., S.-H.W., S.S.H., Y.-S.J.L., and S.C. analyzed data; and S.S.R., Z.Q., S.S.H., S.C., and A.P. wrote the paper.

The authors declare no conflict of interest.

[1]S.S.R. and Z.Q. contributed equally to this work.

[2]Present address: Ion Channels and Sensory Transduction Group, Aix Marseille Université, Centre National de la Recherche Scientifique, Centre de Recherche en Neurobiologie et Neurophysiologie de Marseille, Unite Mixte de Recherche 7286, 13344 Marseille, France.

[3]To whom correspondence may be addressed. E-mail: shuchien@ucsd.edu or ardem@scripps.edu.

This article contains supporting information online at www.pnas.org/lookup/suppl/doi:10.1073/pnas.1409233111/-/DCSupplemental.

PHYSIOLOGY

in vivo. Here we used a genetic strategy to ablate the function of Piezo1 in vivo and show that Piezo1 is a critical component of endothelial cell mechanotransduction.

Results

Piezo1$^{gt/gt}$ Mice Are Embryonic Lethal. To characterize the physiological function of Piezo1, we used a gene trap transgenic line in which a promoter-less β-geo (β-gal and neomycin phosphotransferase) cassette had been randomly integrated in the intron between exons 18 and 19 of the mouse *Piezo1* locus (Fig. 1*A*). The gene trap cassette contains a splice acceptor that co-opts the endogenous splicing of the *Piezo1* transcript, leading to an in-frame fusion protein containing the first 823 residues of Piezo1 and β-geo, a predicted nonfunctional protein. This gene trap allele, *Piezo1^{gt}*, also provides two reporters of Piezo1 expression: β-gal fused to Piezo1 and human placental alkaline phosphatase (PLAP) expressed through an internal ribosome entry site (IRES) (27).

We confirmed proper splicing of the *Piezo1^{gt}* allele by performing RT-PCR with primers targeting the *Piezo1* transcript surrounding the integration site and the start of the gene trap cassette (Fig. S1*A*). We then cloned and expressed the entire *Piezo1^{gt}* transcript in human embryonic kidney (HEK293T) cells (Fig. S1*B*) and found no cellular toxicity in three different assays (Fig. S1*C*). Furthermore, we showed that an N-terminal fragment of Piezo1, Piezo1 (1–823), fused to eGFP did not lead to any MA currents (Fig. S1*D*). These results indicate that *Piezo1^{gt}* would lead to loss of Piezo1 ion channel activity while serving as a reporter of endogenous Piezo1 expression.

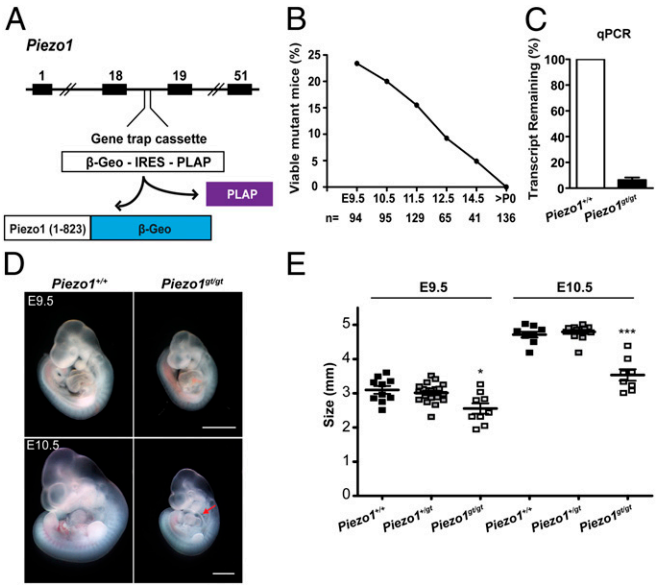

Fig. 1. Piezo1-deficient embryos die at midgestation. (*A*) Diagram of the *Piezo1* genomic locus, gene trap cassette, and the products of *Piezo1* gene trap allele (*Piezo^{gt}*). The exons (black rectangles), β-geo (a fusion between β-gal and neomycin phosphotransferase, blue rectangle), and PLAP (purple rectangle) are indicated. (*B*) Percentage of viable *Piezo1$^{gt/gt}$* mice at different ages derived from *Piezo1$^{gt/+}$* intercrosses. The number of embryos and mice genotyped is shown in the bottom. (*C*) Relative mRNA expression of *Piezo1* in mouse embryonic fibroblasts (MEFs) isolated from E10.5 *Piezo1$^{gt/gt}$* embryos compared with *Piezo1$^{+/+}$* MEFs. mRNA levels were determined by quantitative real-time PCR and normalized to glyceraldehyde 3-phosphate dehydrogenase (*Gapdh*). Bar represents the mean ± SEM ($n = 3$). (*D*) Gross appearance of *Piezo1$^{gt/gt}$* embryos and their *Piezo1$^{+/+}$* littermates. Red arrow indicates pericardial effusion. (Scale bar: 1 mm.) (*E*) Size analysis of representative *Piezo1$^{+/+}$*, *Piezo1$^{+/gt}$*, and *Piezo1$^{gt/gt}$* embryos at E9.5 and E10.5. Numbers of embryos used were *Piezo1$^{+/+}$*, E9.5 ($n = 10$), E10.5 ($n = 9$); *Piezo1$^{+/gt}$*, E9.5 ($n = 20$), E10.5 ($n = 13$); *Piezo1$^{gt/gt}$*, E9.5 ($n = 9$), E10.5 ($n = 8$). Bars represent the mean ± SEM $^*P < 0.05$, $^{***}P < 0.001$, unpaired two-tailed *t* test.

Piezo1$^{+/gt}$ mice were viable and fertile, but intercrossing *Piezo1$^{+/gt}$* mice generated no viable homozygous offspring (Fig. 1*B*). Quantitative PCR (qPCR) analysis using a probe downstream of the gene trap integration site confirmed loss of wild-type *Piezo1* transcript (Fig. 1*C*). *Piezo1$^{gt/gt}$* embryos seemed normal at embryonic day (E) 9, showing a regular heartbeat and blood flow in central vessels, and, at E9.5 major blood vessels such as the dorsal aorta and cardinal veins were present in *Piezo1$^{gt/gt}$* embryos, suggesting that the initial stages of vasculogenesis occurred normally in the absence of Piezo1 function (Fig. S2*A*). However, starting from E9.5, mutant embryos were growth-retarded (Fig. 1 *D* and *E*), and many exhibited pericardial effusion at E10.5, indicative of poor cardiovascular function (28). A majority of *Piezo1$^{gt/gt}$* embryos died at midgestation before E14.5 (Fig. 1*B*).

Piezo1 Expression in Embryonic Endothelial Cells. Embryonic lethality beginning at E9.5 coincides with the development of the cardiovascular system, whose function is required for the survival of the embryo (28). We investigated where Piezo1 is expressed at this time. Piezo1 in situ hybridization probes, an antibody that we had previously generated, as well as commercially available antibodies were not sensitive enough to detect expression of endogenous Piezo1 (18, 29). We therefore used the *Piezo1* promoter-driven β-gal and PLAP reporter genes to analyze the expression pattern of Piezo1. Weak β-gal activity was initially detected at E9 (Fig. S2*B*), when regular heartbeats and blood flow are first established (29). Between E9 and E10.5, β-gal activity increased and was restricted to the developing cardiovascular system, in particular to the vascular endothelium and the inner endocardium surrounding the heart lumen (Fig. 2*A*). Staining of PLAP, a GPI-linked cell surface marker, and platelet/endothelial cell adhesion molecule 1 (PECAM1), an endothelial marker, also confirmed Piezo1 expression in the vascular endothelium (Fig. 2*B*). In the heart, the highest level of X-gal staining at E11.5 was observed in the endothelium lining ventricular outflow tract and atrioventricular canal (Fig. 2*C*), areas predicted to experience strong fluid shear forces generated by blood flow (30, 31).

To provide an even more sensitive method to detect Piezo1 expression, we designed a gene-targeting strategy that would lead to a C-terminus fusion protein of Piezo1 with the fluorescent reporter tdTomato (Fig. S3*A*). Germ-line transmission and successful deletion of the neomycin cassette led to mice that expressed the fluorescent reporter allele *Piezo1$^{P1\text{-}tdT}$* (Fig. S3*B*). RT-PCR analysis of *Piezo1$^{+/P1\text{-}tdT}$* mice confirmed the presence of a fusion allele with the expected size (Fig. S3*C*). Western blot analysis confirmed the presence of a Piezo1 fusion protein in *Piezo1$^{P1\text{-}tdT/P1\text{-}tdT}$* mice (Fig. S3*D*). These mice were viable and expressed Piezo1 in levels similar to *Piezo1$^{+/+}$* controls (Fig. S3*E*).

We then used flow cytometry to detect the epifluorescence of tdTomato with single-cell resolution. We show that PECAM1$^+$ endothelial cells in the embryonic heart and yolk sac of midgestation *Piezo1$^{+/P1\text{-}tdT}$* embryos display a prominent shift in fluorescence peak compared with *Piezo1$^{+/+}$* littermates, indicating expression of the *Piezo1–tdTomato* fusion allele (Fig. 2*D*). We further analyzed cells within the yolk sac that were PECAM1$^-$ as a control (Fig. 2*E*). The majority of yolk sac-derived nonendothelial cells did not show fluorescence above background, confirming our lacZ staining results that Piezo1 is preferentially expressed in endothelial cells. Interestingly, expression of Piezo1 persists in endothelial cells in adult heart, lung, and aorta, as well as in the human umbilical vein endothelial cells (HUVECs) (Fig. S4 *A* and *B*).

Vascular Impairments in Piezo1$^{gt/gt}$ Embryos. Blood flow in mouse embryos begins at E8, and hemodynamic forces from blood flow have been shown to be a critical factor to the development of the

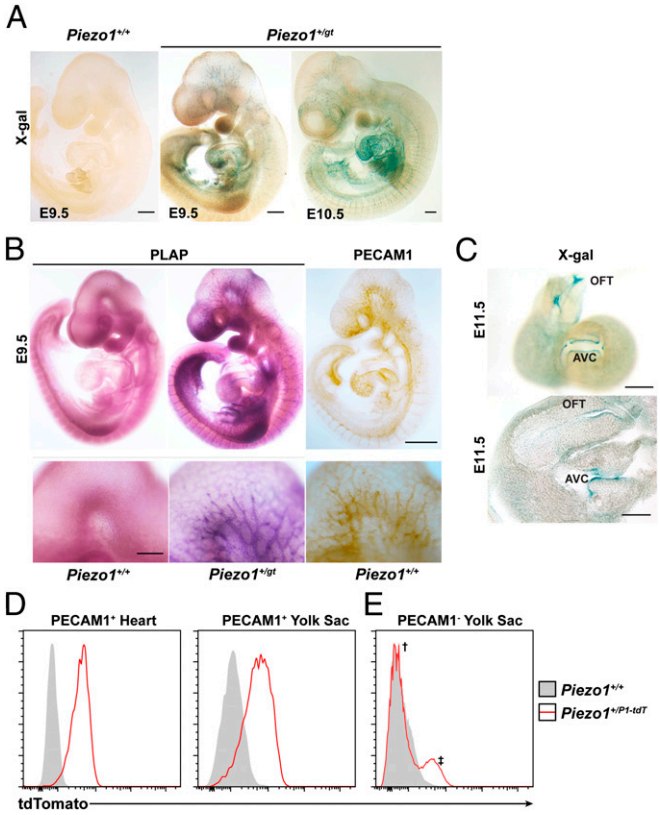

Fig. 2. Piezo1 is expressed in embryonic vascular endothelial cells. (*A*) Representative images of X-gal–stained whole-mount *Piezo1*$^{+/+}$ and *Piezo*$^{+/gt}$ embryos at E9.5 and E10.5. (*B*) Representative image of E9.5 whole-mount *Piezo1*$^{+/+}$ and *Piezo1*$^{+/gt}$ embryos stained for PLAP and PECAM1 and magnification image of embryonic head showing expression of PLAP and PECAM1 from the same embryos. (*C*) Representative images of X-gal–stained E11.5 whole-mount hearts and sections of *Piezo*$^{+/gt}$ embryos. (*D*) Representative histograms of tdTomato fluorescence in PECAM1^{+} cells from *Piezo1*$^{+/+}$ (gray shaded) or *Piezo1*$^{+/P1\text{-}tdT}$ (red line) embryos. E13.5 embryos and E11.5 embryos were used for heart and yolk sac analysis, respectively, owing to technical consideration for tissue preparation. (*E*) Histograms of tdTomato fluorescence in PECAM1^{-} cells from embryos in *D*. †Most PECAM1^{-} cells from *Piezo1*$^{+/tdT}$ yolk sac do not express Piezo1; ‡some PECAM1^{-} cells in *Piezo1*$^{+/tdT}$ yolk sac also express Piezo1-tdTomato. Stainings in *A*–*C* were performed in at least four embryos per genotype per time point. Histograms in *D* and *E* are representative of at least two embryos per genotype. [Scale bars: 400 μm (*A*), 500 μm and 200 μm, respectively (*B*), and 200 μm (*C*).]

refined vascular network (32, 33). The initial stage of vascular remodeling relies entirely on endothelial cells because mural cells consisting of smooth muscle cells and pericytes present in mature vessels are not recruited until after the primary vessel structure has been established (34). Having shown that Piezo1 is expressed in embryonic endothelial cells, we characterized the morphology of the developing vascular system of Piezo$^{gt/gt}$ mice.

We performed H&E staining and PECAM1 immunostaining to observe vessel morphology in the yolk sac and the embryo proper from E8.5 to E10.5, when vascular remodeling and network formation occur. PECAM1 staining of E8.5 yolk sac shows that the organization of the early vascular plexus is significantly altered in *Piezo1*$^{gt/gt}$ yolk sacs (Fig. 3 *A* and *B*). The layer of endothelial cells that cover the mesodermal cells of the yolk sac is wider in *Piezo1*$^{gt/gt}$ embryos, and the vasculature is delayed in its organization of major vessels. By E9.5, the yolk sac vasculature is less defined and the number of major vessels is fewer relative to littermate controls (Fig. S5*A*). H&E staining of a cross-section of the E9.5 yolk sac shows that wild-type yolk sacs have a wide distribution of small- and large-diameter vessels, whereas *Piezo1*$^{gt/gt}$ yolk sacs lack major vessels (Fig. 3 *C* and *D*). Vascular remodeling in the *Piezo1*$^{gt/gt}$ embryo proper reveals a similar lack of vessel organization at E9.5 and a significant decrease in the number of major vessels at E10.5 compared with *Piezo1*$^{+/+}$ littermate controls (Fig. 5*SB*). Histological analysis of the heart at E8.5 did not reveal obvious morphological differences between *Piezo1*$^{gt/gt}$ embryos and littermate controls (Fig. 5*SC*). These data indicate a role for Piezo1 in the remodeling of the embryonic vasculature and suggest that a loss of functional Piezo1 leads to an impairment of mechanotransduction processes in vivo.

Piezo1 Is Activated by Shear Stress. We have previously shown that Piezo1 is activated by two types of distinct mechanical stimulations: by the indentation of a cell with a glass probe and by stretching the cell membrane (18). Although membrane stretch can affect endothelial cells, fluid shear stress represents the most relevant force experienced by endothelial cells (35, 36). We tested shear stress activation of Piezo1 using electrophysiology. We used a perfusion tube and subjected cells to laminar flow shear stress by applying 600-ms pulses of solution flow directed on to the recording cell (Fig. 4*A*). Whole-cell inward currents (I_{max}: −533 ± 64 pA) could be recorded from Piezo1-IRES-eGFP transfected HEK293T cells when stimulated by shear stress in the intensity range of 52 ± 3–64 ± 2 dynes/cm^2, but not from IRES-eGFP transfected cells (I_{max}: −8.7 ± 1.3 pA) even up to 70 dynes/cm^2 (Fig. 4*B*). The pressure applied to the solution was correlated to shear stress by using the particle image velocimetry method to estimate the shear stress intensity at the cell surface (37). For pressure pulses ranging from 10 mmHg to 60 mmHg, the average bead velocity ranged from 6.9 ± 0.6 μm/ms to 21.0 ± 1.3 μm/ms, and the estimated wall shear stress intensity ranged from 23.3 ± 2.2 dynes/cm^2 to 70.2 ± 4.2 dynes/cm^2 (Fig. 4*C*). The half-maximal activation intensity for Piezo1 was measured to be 57 ± 3 dynes/cm^2 (Fig. 4*D*). Similar to MA currents, shear stress-activated Piezo1 channel currents inactivate in continued presence of stimulus, but with a slower time constant

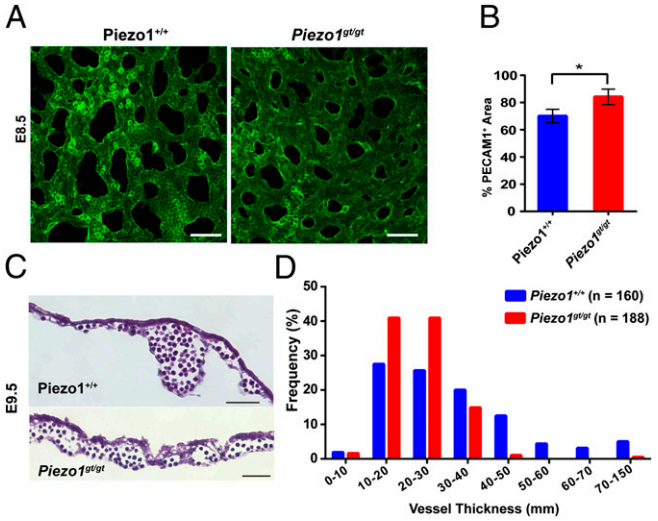

Fig. 3. Piezo1-deficient embryos display vascular remodeling defects. (*A*) Representative images of PECAM1-stained E8.5 *Piezo1*$^{+/+}$ and *Piezo1*$^{gt/gt}$ whole-mount yolk sacs. (*B*) Quantification of PECAM1^{+} area in E8.5 *Piezo1*$^{+/+}$ and *Piezo1*$^{gt/gt}$ whole-mount yolk sac from $n = 3$ experiments. (*C*) Representative H&E staining of E9.5 yolk sac cross-sections from *Piezo1*$^{+/+}$ and *Piezo1*$^{gt/gt}$ embryos. (*D*) Quantification of vessel thickness from H&E staining of E9.5 yolk sac from $n = 2$ experiments. *$P < 0.05$, unpaired two-tailed Student *t* test. [Scale bars: 100 μm (*A*) and 200 μm (*C*).]

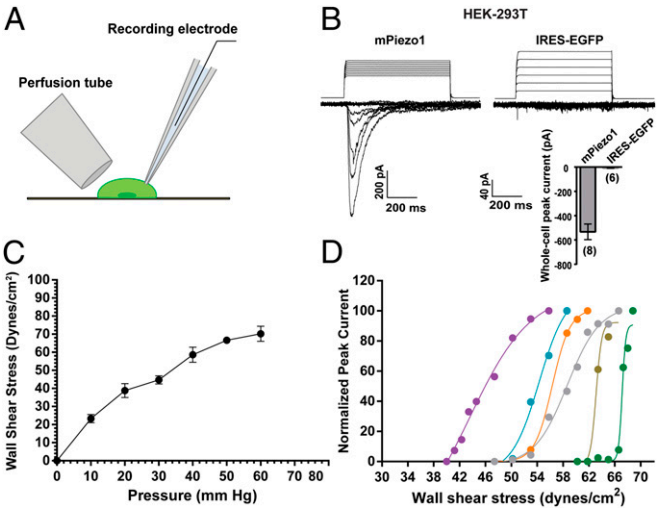

Fig. 4. Piezo1 is activated by fluid shear stress. (*A*) Pictorial representation of perfusion tube setup. Whole-cell currents were recorded from HEK293T cells while the cell was stimulated by shear stress induced by directing pulses of fluid flow through a perfusion tube placed relative to the cell. The flow rate is regulated by varying the pressure applied to the fluid inside the tube. (*B*) Representative traces of whole-cell currents recorded at −80 mV from HEK293T cells expressing mPiezo1 (*Left*) or IRES-eGFP (*Right*) in response to 600-ms pulses of increasing laminar shear stress. The stimulus trace above the current indicates the pressure pulse applied to the solution in the perfusion tube (which was later back-calculated to the applied shear stress intensities) and corresponds to the whole-cell current recorded for that stimulus. (*Inset*) Shear stress-induced average maximum whole-cell peak currents from mPiezo1 ($n = 8$) and IRES-EGFP ($n = 6$) transfected cells. Bars indicate mean ± SEM. (*C*) Pressure–wall shear stress relationship. Particle image velocimetry was used to estimate the wall shear stress intensity at the indicated tube pressure. Each data point is the mean ± SEM from values of five or six independent trials. The measurement was done for the range of pressure (0–60 mmHg) used to activate the cells during the experiment. (*D*) Wall shear stress to normalized peak current relationship plotted for six individual cells expressing mPiezo1, depicting range of activation. For each cell, currents were normalized to the peak current recorded at maximum shear stress, before losing the seal. The stimulus–response curve was fit with a Boltzmann function to determine the half-maximal response.

of 65.6 ± 9.0 ms ($n = 8$). Interestingly, it has been recently shown that stretch-induced Piezo1 inactivation kinetics can vary dramatically in different cell types, supporting the possibility that laminar shear stress (LS) can also modulate Piezo1 activity (38). Furthermore, physiologically relevant fluid shear stress from blood flow comes in many forms, including laminar and disturbed flow. Disturbed flow during embryogenesis and in the adult is common in arterial branch points. As a rapidly adapting ion channel, disturbed flow would allow recovery of Piezo1 and could activate the channel repeatedly. Overall, these data show that Piezo1 can be activated by fluid shear stress, as well as by membrane indentation and stretch.

Piezo1 Is Involved in Endothelial Cell Alignment Under Flow. The ability of endothelial cells to align in the direction of fluid flow is one of the best-studied cellular consequences of mechanotransduction (39). To determine whether loss of PIEZO1 leads to defects in morphology of vascular endothelial cells and its responsiveness to shear flow, we compared the LS-induced remodeling in HUVECs transfected with siRNA for PIEZO1 and scrambled siRNA. HUVECs were subjected to shear stress (12 dynes/cm^2) for 24 h and examined for changes in cellular morphology. qPCR analysis revealed ∼80% knockdown of PIEZO1 transcript in PIEZO1 siRNA cells compared with scrambled siRNA (Fig. S6*A*). The relatively long duration and the level of shear stress were chosen based on previous studies on shear-induced remodeling of HUVECs (40).

Stress fibers visualized by F-actin immunostaining and their orientation angles show impaired alignment in PIEZO1 siRNA cells compared with scrambled siRNA (Fig. 5*A*). For HUVECs transfected with scrambled siRNA (Fig. 5 *B* and 5 *C*, *Left*), neither the stress fibers nor the cells showed any preferential orientation under static condition (ST), but both showed dominant orientations parallel to the flow direction (0°) under LS, with 41 ± 0.58% of the stress fibers and 54 ± 0.38% of the cells having orientations within the range of ± 15°. Transfection of HUVECs with siRNA for PIEZO1 (Fig. 5 *B* and *C*, *Right*) caused significant decreases in the LS-induced orientations of stress fibers (25 ± 0.71%) and cells (31 ± 1.30%) in comparison with scrambled siRNA under LS. Morphological determination of cell elongation in scrambled siRNA cells showed that LS caused an increase in aspect ratio to 3.3 ± 0.07 from the ST value of 2.0 ± 0.04 (Fig. S6*B*, *Left*). Cells transfected with PIEZO1 siRNA showed a reduction in the LS-induced elongation, with an aspect ratio (2.6 ± 0.08) significantly lower than that with scrambled siRNA, whereas the ST value of 2.1 ± 0.04 is not significantly different (Fig. S6*B*, *Right*). It is worth noting that we observe a role for Piezo1 in alignment and elongation in response to lower forces of shear stress compared with forces needed to activate Piezo1 in studies of electrophysiology. This is not surprising, because the 24-h time frame of the experiments involving altered cell morphology allows accumulation of low-level cation influx. These observations indicate that knocking down PIEZO1 results in significant decreases in the mechanosensitivity of the endothelial cells in terms of alignment and elongation in response to LS. However, the dependence on PIEZO1 is partial, and it is likely that other factors also contribute to the shear stress-dependent alignment and elongation.

Discussion

Vascular development and cardiogenesis in the mouse embryo is influenced by hemodynamic forces owing to blood flow. For example, vascular remodeling in the yolk sac is compromised when cardiac function/output is reduced or absent (41). Surgical ligation of the left arch arteries in mouse embryos prevents normal blood flow and leads to abnormal regression and an accompanying enlargement of the right arteries (42). In addition, local hemodynamic shear stress forces imparted on vascular endothelial cells of developing blood vessels are necessary and sufficient to induce remodeling in the mouse yolk sac (43). These data suggest that disruption of mechanotransduction in the cardiovascular system during the time when blood flow initiates around E8–E9 is expected to cause a defect in vascular development.

The direct effect of hemodynamic force on endothelial cells during vascular remodeling is not well understood. In response to fluid shear stress in vitro, endothelial cells change their gene expression profiles and can realign their cytoskeletal structure (35). Putative mechanotransducers have been identified from cultured endothelial cells or in the mature vasculature, including ion channels (44, 45), the apical glycocalyx (46), cytoskeleton (47), primary cilia (48), and a protein complex comprising PECAM1, vascular endothelial cadherin, and vascular endothelial growth factor receptor 2 (VEGFR2) (49). Ion channels such as TREK-1 have been shown to be activated by stretch and shear stress (50). However, the identity of the shear stress sensor or sensors during embryogenesis has been unknown. Our data reveal that Piezo1 is expressed in embryonic endothelial cells and that Piezo1 deficiency leads to disruption of vascular development in the mouse embryo and yolk sac. In addition, our results provide evidence that Piezo1 is a sensor of shear stress, and that endothelial cell alignment in response to shear stress is

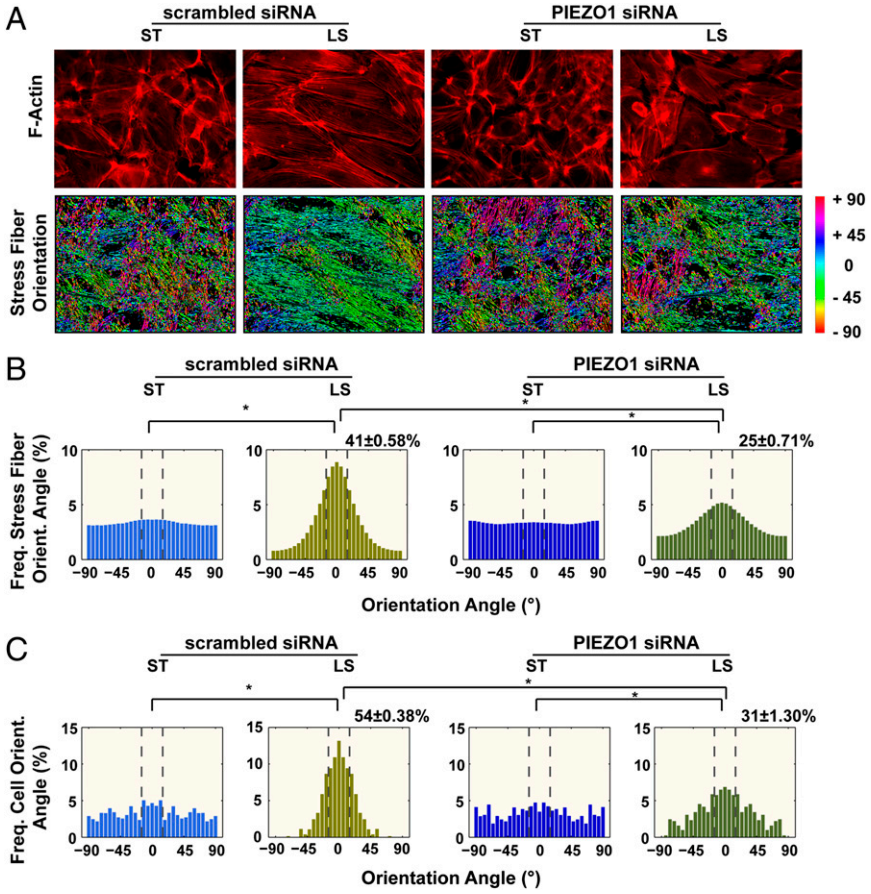

Fig. 5. Knockdown of PIEZO1 leads to defects in cellular alignment upon laminar shear stress. (*A*) F-actin images stained with TRITC-phalloidin (*Upper*) and angles of stress fiber orientation (*Lower*). Angle measurements were assigned a color code (right) where 0° is parallel to the flow chamber and −90° and 90° are perpendicular. (*B*) Histograms of stress fiber orientation of cells. (*C*) Histograms of cell orientation. The mean ± SEM values refer to percentage of orientations between ±15° for three independent biological experiments. Total numbers of cells analyzed are 348 (ST) and 236 (LS) for scrambled siRNA and 290 (ST) and 170 (LS) for PIEZO1 siRNA. ST, static; LS, laminar shear for 24 h. Asterisk indicates significant difference by Watson's U2 test.

compromised in the absence of Piezo1. It is possible that incomplete endothelial cell alignment in response to shear stress during remodeling of arteries leads to the vascular remodeling defects observed in Piezo1-deficient embryos. Alternatively, Piezo1-dependent calcium influx could modulate multiple downstream signaling pathways and influence vascular remodeling through pleiotropic mechanisms. Future studies with conditional knockouts will address whether endothelium and/or other cell types are dependent on Piezo1-signaling in the embryo and in the mature cardiovascular system.

Materials and Methods

All animal procedures were approved by The Scripps Research Institute's Institutional Animal Care and Use Committee. Detailed methods are provided in *SI Materials and Methods*.

X-gal and PLAP Stainings. Stainings were performed following standard procedures. For X-gal staining, embryos were washed in X-gal washing buffer (PBS with 2 mM $MgCl_2$, 0.02% Nonidet P-40, and 0.01% sodium deoxycholate), incubated in X-gal staining buffer (X-gal washing buffer with 5 mM potassium ferricyanide, 5 mM potassium ferrocyanide, and 1 mg/mL X-gal) overnight with gentle shaking at 37 °C, and then postfixed in neutral buffered 10% (vol/vol) formalin. Whole-mount embryos and tissues labeled with X-gal were cleared in a 1:1 mixture of benzyl alcohol:benzyl benzoate clearing and imaged under Nikon SMZ1500 stereomicroscope (51). Images were obtained under Olympus AX70 microscope.

For PLAP staining, fixed embryos were heat-inactivated in PBS for 1.5 h at 65 °C and washed in buffer B1 [0.15 M NaCl and 0.1 M Tris·HCl (pH7.5)] and buffer B3 [0.1 M NaCl, 50 mM $MgCl_2$, and 0.1 M Tris·HCl (pH 9.5)] sequentially. Embryos were then incubated in NBT/BCIP solution (Roche) at room temperature overnight and postfixed. Images were obtained under Nikon SMZ1500 stereomicroscope.

Flow Cytometry Analysis. Hearts and yolk sacs were isolated from embryos generated from timed matings between *Piezo1*$^{+/P1\text{-}tdT}$ mice. Yolk sacs and hearts were minced and incubated with 0.5 mg/mL collagenase type IV, 0.1 mg/mL DNaseI, and 1 mg/mL trypsin inhibitor at 37 °C for 30 min, being pipetted repeatedly several times throughout the incubation. The samples were washed with FACS buffer [PBS containing 2% (vol/vol) FBS and 2 mM EDTA] and centrifuged at 500 × *g* for 5 min. Erythrocytes were then lysed using a multispecies RBC lysis buffer (eBioscience) for 5 min at room temperature, then washed again with FACS buffer. The cells were then resuspended in FACS buffer, filtered through 100-μm-diameter nylon mesh, and incubated with FcBlock (BD) for 5 min at room temperature. They were then stained with an APC anti-PECAM1 antibody (BD) for 15 min at 4 °C in the dark. The cells were washed once then resuspended in FACS buffer for data acquisition using a BD LSRII flow cytometer. Data were analyzed using FlowJo (TreeStar).

LS Stimulation. Shear stress was applied using a perfusion tube (borosilicate glass capillary, pulled to an inner diameter 17 μm at the mouth) that was filled with extracellular solution (same as bath solution) and was positioned at an angle of 30° (sensapex SMX-series micromanipulation system; Warner Instruments) relative to the cell. The micromanipulator was used to control the position of the perfusion tube and maintain consistency between each trial. A Clampex 10.2 controlled pressure clamp HSPC-1 devise (ALA Scientific) was connected to the perfusion tube and was used to apply pressure on the solution to generate 600-ms pulses of flow. Starting from 0 mmHg, increasing increments of 20 mmHg pressure was applied every 20 s

PHYSIOLOGY

to raise the flow rate with each progressive pulse. Once a whole-cell inward current response was detected at a certain pressure level, the increments were reduced to 2 mmHg and the protocol was run again, starting from the lowest stimulus that elicited the initial response, to obtain a more accurate and sensitive stimulus–response curve for each cell. This data were then used to obtain activation range and half-maximal activation values.

Laminar Flow Experiments for Cellular Alignment. HUVECs were seeded on glass slides coated with 50 μg/mL collagen-1 1 d before the experiment. The slide was assembled into the flow chamber and exposed to laminar shear at a wall shear stress of 12 dynes/cm^2. The cells obtained under static condition were used as concurrent control groups. During the flow experiment, the system was kept at 37 °C and pH 7.5.

ACKNOWLEDGMENTS. We thank Taryn Goode for embryo analysis, Sergey Kupriyanov and Greg Martin at The Scripps Research Institute Mouse Genetics Core for embryonic stem cell injections, James Watson and Terri Johnson for histology support, Kathy Spencer for help with imaging, and Dr. Hugh Rosen for mCherry antibody. This work was supported by National Institutes of Health Grants R01 DE022358 (to A.P.) and 1R01HL121365 (to S.C.). S.S.R. is the recipient of a predoctoral fellowship from the California Institute for Regenerate Medicine. B.C. is the recipient of a postdoctoral fellowship from Dorris Neuroscience Center.

1. Hoffman BD, Grashoff C, Schwartz MA (2011) Dynamic molecular processes mediate cellular mechanotransduction. *Nature* 475(7356):316–323.
2. Gillespie PG, Müller U (2009) Mechanotransduction by hair cells: Models, molecules, and mechanisms. *Cell* 139(1):33–44.
3. Tsunozaki M, Bautista DM (2009) Mammalian somatosensory mechanotransduction. *Curr Opin Neurobiol* 19(4):362–369.
4. Orr AW, Helmke BP, Blackman BR, Schwartz MA (2006) Mechanisms of mechanotransduction. *Dev Cell* 10(1):11–20.
5. Jaalouk DE, Lammerding J (2009) Mechanotransduction gone awry. *Nat Rev Mol Cell Biol* 10(1):63–73.
6. Hahn C, Schwartz MA (2009) Mechanotransduction in vascular physiology and atherogenesis. *Nat Rev Mol Cell Biol* 10(1):53–62.
7. Chalfie M (2009) Neurosensory mechanotransduction. *Nat Rev Mol Cell Biol* 10(1): 44–52.
8. Corey DP, Hudspeth AJ (1979) Response latency of vertebrate hair cells. *Biophys J* 26(3):499–506.
9. Guharay F, Sachs F (1984) Stretch-activated single ion channel currents in tissue-cultured embryonic chick skeletal muscle. *J Physiol* 352:685–701.
10. Delmas P, Hao J, Rodat-Despoix L (2011) Molecular mechanisms of mechanotransduction in mammalian sensory neurons. *Nat Rev Neurosci* 12(3):139–153.
11. Nilius B, Honoré E (2012) Sensing pressure with ion channels. *Trends Neurosci* 35(8): 477–486.
12. Arnadottir J, Chalfie M (2010) Eukaryotic mechanosensitive channels. *Annu Rev Biophys* 39:111–137.
13. Geffeney SL, Goodman MB (2012) How we feel: Ion channel partnerships that detect mechanical inputs and give rise to touch and pain perception. *Neuron* 74(4):609–619.
14. Yan Z, et al. (2013) Drosophila NOMPC is a mechanotransduction channel subunit for gentle-touch sensation. *Nature* 493(7431):221–225.
15. Walker RG, Willingham AT, Zuker CS (2000) A Drosophila mechanosensory transduction channel. *Science* 287(5461):2229–2234.
16. O'Hagan R, Chalfie M, Goodman MB (2005) The MEC-4 DEG/ENaC channel of Caenorhabditis elegans touch receptor neurons transduces mechanical signals. *Nat Neurosci* 8(1):43–50.
17. Dedman A, et al. (2009) The mechano-gated K(2P) channel TREK-1. *Eur Biophys J* 38(3):293–303.
18. Coste B, et al. (2010) Piezo1 and Piezo2 are essential components of distinct mechanically activated cation channels. *Science* 330(6000):55–60.
19. Coste B, et al. (2012) Piezo proteins are pore-forming subunits of mechanically activated channels. *Nature* 483(7388):176–181.
20. Kim SE, Coste B, Chadha A, Cook B, Patapoutian A (2012) The role of Drosophila Piezo in mechanical nociception. *Nature* 483(7388):209–212.
21. Woo SH, et al. (2014) Piezo2 is required for Merkel-cell mechanotransduction. *Nature* 509(7502):622–626.
22. Maksimovic S, et al. (2014) Epidermal Merkel cells are mechanosensory cells that tune mammalian touch receptors. *Nature* 509(7502):617–621.
23. Ikeda R, et al. (2014) Merkel cells transduce and encode tactile stimuli to drive aβ-afferent impulses. *Cell* 157(3):664–675.
24. Albuisson J, et al. (2013) Dehydrated hereditary stomatocytosis linked to gain-of-function mutations in mechanically activated PIEZO1 ion channels. *Nat Commun* 4: 1884.
25. Gallagher PG (2013) Disorders of red cell volume regulation. *Curr Opin Hematol* 20(3): 201–207.
26. Coste B, et al. (2013) Gain-of-function mutations in the mechanically activated ion channel PIEZO2 cause a subtype of Distal Arthrogryposis. *Proc Natl Acad Sci USA* 110(12):4667–4672.
27. Leighton PA, et al. (2001) Defining brain wiring patterns and mechanisms through gene trapping in mice. *Nature* 410(6825):174–179.
28. Conway SJ, Kruzynska-Frejtag A, Kneer PL, Machnicki M, Koushik SV (2003) What cardiovascular defect does my prenatal mouse mutant have, and why? *Genesis* 35(1): 1–21.
29. Faucherre A, Nargeot J, Mangoni ME, Jopling C (2013) Piezo2b regulates vertebrate light touch response. *J Neurosci* 33(43):17089–17094.
30. Hove JR, et al. (2003) Intracardiac fluid forces are an essential epigenetic factor for embryonic cardiogenesis. *Nature* 421(6919):172–177.
31. Santhanakrishnan A, Miller LA (2011) Fluid dynamics of heart development. *Cell Biochem Biophys* 61(1):1–22.
32. McGrath KE, Koniski AD, Malik J, Palis J (2003) Circulation is established in a stepwise pattern in the mammalian embryo. *Blood* 101(5):1669–1676.
33. le Noble F, et al. (2004) Flow regulates arterial-venous differentiation in the chick embryo yolk sac. *Development* 131(2):361–375.
34. Walls JR, Coultas L, Rossant J, Henkelman RM (2008) Three-dimensional analysis of vascular development in the mouse embryo. *PLoS ONE* 3(8):e2853.
35. Chien S (2007) Mechanotransduction and endothelial cell homeostasis: The wisdom of the cell. *Am J Physiol Heart Circ Physiol* 292(3):H1209–H1224.
36. Culver JC, Dickinson ME (2010) The effects of hemodynamic force on embryonic development. *Microcirculation* 17(3):164–178.
37. Willert CE, Gharib M (1991) Digital particle image velocimetry. *Exp Fluids* 10(4): 181–193.
38. Peyronnet R, et al. (2013) Piezo1-dependent stretch-activated channels are inhibited by Polycystin-2 in renal tubular epithelial cells. *EMBO Rep* 14(12):1143–1148.
39. Davies PF (1995) Flow-mediated endothelial mechanotransduction. *Physiol Rev* 75(3): 519–560.
40. Hahn C, Wang C, Orr AW, Coon BG, Schwartz MA (2011) JNK2 promotes endothelial cell alignment under flow. *PLoS ONE* 6(8):e24338.
41. Huang C, et al. (2003) Embryonic atrial function is essential for mouse embryogenesis, cardiac morphogenesis and angiogenesis. *Development* 130(24):6111–6119.
42. Yashiro K, Shiratori H, Hamada H (2007) Haemodynamics determined by a genetic programme govern asymmetric development of the aortic arch. *Nature* 450(7167): 285–288.
43. Lucitti JL, et al. (2007) Vascular remodeling of the mouse yolk sac requires hemodynamic force. *Development* 134(18):3317–3326.
44. O'Neil RG, Heller S (2005) The mechanosensitive nature of TRPV channels. *Pflugers Arch* 451(1):193–203.
45. Yamamoto K, et al. (2006) Impaired flow-dependent control of vascular tone and remodeling in P2X4-deficient mice. *Nat Med* 12(1):133–137.
46. Thi MM, Tarbell JM, Weinbaum S, Spray DC (2004) The role of the glycocalyx in reorganization of the actin cytoskeleton under fluid shear stress: A "bumper-car" model. *Proc Natl Acad Sci USA* 101(47):16483–16488.
47. Mammoto A, Mammoto T, Ingber DE (2008) Rho signaling and mechanical control of vascular development. *Curr Opin Hematol* 15(3):228–234.
48. AbouAlaiwi WA, et al. (2009) Ciliary polycystin-2 is a mechanosensitive calcium channel involved in nitric oxide signaling cascades. *Circ Res* 104(7):860–869.
49. Tzima E, et al. (2005) A mechanosensory complex that mediates the endothelial cell response to fluid shear stress. *Nature* 437(7057):426–431.
50. Patel AJ, et al. (1998) A mammalian two pore domain mechano-gated S-like K+ channel. *EMBO J* 17(15):4283–4290.
51. Schatz O, Golenser E, Ben-Arie N (2005) Clearing and photography of whole mount X-gal stained mouse embryos. *Biotechniques* 39(5):650, 652, 654 passim.